Choroidal Thickness in Patients With Reticular Pseudodrusen Using 3D 1060-nm OCT Maps

Paulina Haas,[1] Marieh Esmaeelpour,[1,2] Siamak Ansari-Shahrezaei,[1] Wolfgang Drexler,[2] and Susanne Binder[1]

[1]Ludwig Boltzmann Institute for Retinology and Biomicroscopic Laser Surgery, Department of Ophthalmology, Rudolph Foundation Clinic, Vienna, Austria
[2]Center for Medical Physics and Biomedical Engineering, Medical University Vienna, Vienna, Austria

Correspondence: Marieh Esmaeelpour, Department of Ophthalmology, Rudolph Foundation Clinic, Juchgasse 25, 1030 Vienna, Austria; marieh.esmaeelpour@meduniwien.ac.at.

Submitted: September 26, 2013
Accepted: March 9, 2014

Citation: Haas P, Esmaeelpour M, Ansari-Shahrezaei S, Drexler W, Binder S. Choroidal thickness in patients with reticular pseudodrusen using 3D 1060-nm OCT maps. *Invest Ophthalmol Vis Sci*. 2014;55:2674–2681. DOI:10.1167/iovs.13-13338

Purpose. To map and analyze choroidal thickness (ChT) in AMD patients with reticular pseudodrusen (RPD) using three-dimensional (3D) 1060-nm optical coherence tomography (OCT).

Methods. Fifty eyes from 25 patients with RPD were grouped according to the severity of AMD and the presence of RPD. All patients were imaged by high-speed (60,000 A-scans/s) 3D 1060-nm OCT over a 36 × 36° field of view. Choroidal thickness maps were automatically generated and compared with RPD areas visualized by fundus autofluorescence and infrared imaging. Retinal thickness maps, ChT maps, Haller's and Sattler's layer thickness were statistically analyzed between groups.

Results. The mean ± SD (micrometers) subfoveal ChT was 201 ± 88 μm, 145 ± 48 μm, and 271 ± 130 μm for dry AMD with RPD, wet AMD with RPD, and eyes with wet AMD and no RPD, respectively. Choroidal thickness maps demonstrated the most significant choroidal thinning within eyes with wet AMD and RPD. Sattler's and Haller's layer thickness differed across the Early Treatment Diabetic Retinopathy Study grid when compared between eyes with and without RPD. Within eyes with RPD, ChT maps visualized that ChT was thicker below RDP areas than non-RPD areas.

Conclusions. The 3D 1060-nm OCT choroidal maps over a large field of view offer noninvasive visualization for demonstrating local thickening correlation with RPD within each eye and overall thinning owing to AMD severity and RPD. This choroidal thinning was most striking in Sattler's layer, suggesting a choroidopathy of this vascular layer.

Keywords: age-related macular degeneration, optical coherence tomography, choroidal thickness maps, retina, choroidal neovascularization

The first unified imaging description of reticular pseudodrusen (RPD) was presented as a hallmark of a complex disease process in AMD in association with RPE and choroidal changes.[1] Accumulations of extracellular debris deposits are called drusen and are best differentiated by multimodal imaging.[1,2] Drusen are distinguished by their localization and morphology into cuticular, soft, and subretinal drusenoid deposits.[2] While RPD are subretinal drusenoid deposits, cuticular and soft drusen are located below RPE. Drusen number and size are used to classify and to assess the risk of developing advanced AMD.[3,4] Although RPD were described as early as 1990,[5] they are not part of the current classification system because of a broad use of fundus photography for clinical examinations.[3,4] In AMD, the presence of RPD is associated with pathogenic progression such as in outer retinal loss[6] and acquired vitelliform detachments.[7] In eyes with geographic atrophy, RPD have a prevalence of approximately 60% to 90%.[8,9] The risk of conversion to choroidal neovascularization (CNV) is highly increased if RPD are present.[10–12]

Many studies have since related RPD to choroidal thickness (ChT) alteration, atrophy, and fibrosis.[10,13–16] The choroid is thickest 3000 μm superior to the fovea position in eyes with RPD.[15] Thinner choroids were found when choroidal segments below RPD areas were compared with the same areas in controls without any retinal disease.[16] In contrast, the statistical significance of thinner choroids in RPD eyes was diminished by adjusting thickness measurements for age and sex when compared with those with AMD without RPD.[17] Reticular pseudodrusen is found mostly at the superior or at the superior temporal arcade[15,16,18] and has been associated with choroidal watershed zones.[16] However, the choroid is thicker superiorly than inferiorly in both eyes with early AMD and in eyes with RPD,[15] and there may be no significant relationship between ChT and RPD in this region. Previous studies using optical coherence tomography (OCT) to measure ChT in eyes with RPD were limited by the number of scans and the area size of segmentation to view overall ChT distribution and relate RPD distribution within each eye.

The present study investigates ChT in eyes with AMD and RPD by a choroidal penetration three-dimensional (3D) 1060-nm OCT and automatic ChT mapping over a large field of view. Maps are statistically analyzed with regard to the distribution of ChT and RPD and the severity of AMD defined by the Age-Related Eye Disease Study (AREDS).[19]

Table 1. Subfoveal ChT, Age, and AL Distribution With Different AMD Severities and the Presence of RPD

AMD Severities	Nonneovascular With RPD	Neovascular With RPD	Neovascular With No RPD
Foveal thickness, μm (range)	222 ± 47* (119–269)	433 ± 186 (120–707)	386 ± 139 (175–695)
Subfoveal ChT, μm (range)	201 ± 88 (76–415)	145 ± 48† (78–240)	271 ± 130† (127–432)
Age, y	77 ± 10	80 ± 7	76 ± 11
AL, mm	23.32 ± 1	23.5 ± 0.9	22.72 ± 0.9
RPD distribution	80% Superior 60% Inferior 60% Nasal 50% Temporal	80% Superior 65% Inferior 50% Nasal 50% Temporal	No RPD

* $P < 0.001$.
† $P < 0.01$; one-way ANOVA, post hoc $P < 0.05$.

Methods

Study Population

Twenty-five patients were recruited for this study. Written informed consent was obtained from the subjects after explanation of the nature and possible consequences of the study prior to enrollment. The research adhered to the tenets of the Declaration of Helsinki. Ethical approval was obtained prospectively from the Institutional Review Board "The Ethical Commission of Vienna."

All patients (17 female and 8 male Caucasians; mean age 77.5 years; range, 58–91 years) were thoroughly examined, including best-corrected visual acuity (measured using the Early Treatment Diabetic Retinopathy Study [ETDRS] chart), fundus autofluorescence (FAF) and infrared (IR) imaging, commercial high-definition OCT at approximately 800-nm wavelength (Cirrus; Carl Zeiss Meditec, Dublin, CA, USA), and fluorescein and indocyanine green angiography (angiography only when clinically indicated based on ethical issues). They were included if at least one eye was diagnosed with AMD, and RPD were seen on scanning laser ophthalmoscope imaging with infrared or FAF, with a definite RPD appearance of deposits above the RPE on the 800-nm OCT in corresponding locations. Only eyes with AMD lesions such as medium to large drusen (five or more), geographic atrophy (GA), or CNV in the fovea or within the foveal rim were included. Reticular pseudodrusen was defined as a regular network of uniform round or oval irregularities with a diameter ranging between 50 and 400 μm, corresponding to hypofluorescent spots (with a hyperfluorescent halo) on FAF imaging. On IR images, RPD were identified as a pattern-like grouping of ill-defined lesions with a decreased reflectivity. Exclusion criteria included myopia > 6 diopters, history of glaucoma, any cause of media opacities resulting in impaired visualization of the macula, hereditary diseases, polypoidal choroidal vasculopathy or secondary CNV due to pathologic myopia (≥2 diopters, spherical equivalent), angioid streaks, inflammatory or infectious chorioretinal disease, serious trauma, diabetic retinopathy, and systemic acute inflammatory or infectious disease.

All patients enrolled in the present study were classified according to the clinical and, if available, also angiographic findings (non-CNV AMD; AMD including predominantly classic CNV, minimal classic CNV, occult CNV, and retinal angiomatous proliferation).[19]

OCT Imaging and Thickness Maps

High-speed, 60,000 A-scans/s, 3D OCT imaging at 1060 nm was performed with less than 2.5 mW at the cornea, well below the maximum power limit for 10-second exposure,[20,21] with a spectral-domain optical coherence tomography (SD-OCT) prototype manufactured by the Drexler laboratory. Three-dimensional OCT volumes for ChT mapping were acquired at 1060-nm wavelength with 15- to 20-μm transverse resolution, approximately 7-μm axial resolution and 512 voxels per depth-scan (A-scan). Raster scans across a 36 × 36° field were centered on the fovea and resulted in up to 120 frames/s. Another 3D 1060-nm OCT volume was focused roughly on the RPD area with a 12 × 12° field of view to obtain details of the RPD and choroidal stroma appearance. Three-dimensional 1060-nm OCT images were then studied thoroughly for RPD, choroidal stroma variations, and vascular changes. Viewing RPD with a 1060-nm wavelength light source is new, and images were compared with 800-nm OCT images to validate the similarity of RPD appearance. System specifications of both OCT instruments (800 and 1060 nm) such as ~97 dB signal-to-noise ratio and their roll-off with scanning depth of 6 dB at ~1.1 mm, ~6- to 7-mm axial resolution, and 2.6-mm scanning depth were comparable to allow an objective and fair comparison of the wavelength effect of RPD visualization performance. Imaging with 800-nm OCT was performed over a field of view of 20° centered on the fovea with 512 × 512 A-scans and 128 B-scans. Images were processed and registered for eye movements, denoising, and contrast improvement with ImageJ software (provided in the public domain by National Institutes of Health, Bethesda, MD, USA; http://rsb.info.nih.gov/ij/index.html)[22] and the "Neat Video" plugin in VirtualDub (provided in the public domain at http://www.virtualdub.org/ by Free Software Foundation, Inc., Cambridge, MA, USA). Tomograms of each OCT device were viewed with ImageJ software. For comparison of the OCT images at two different wavelengths, enface images of the OCT volumes were used to help in identifying scans at the same locations. For the investigation of the ChT variation throughout the entire field of view, ChT maps were generated based on automatic segmentation.[23] Automatic retinal and choroidal segmentation, automatic measurement of subfoveal ChT, and the generation of thickness maps were used for this purpose and are described elsewhere.[23,24] Briefly, this method uses training data from manual segmentations in healthy and diseased eyes to build a statistical model. Its advantage is that it can actively learn and determine the segmentation line in a low signal, noisy environment such as in OCT tomograms in the region of the choroid without having to rely on boundary edge information. The resulting pixel distance was converted into optical distance using the depth-sampling calibration for the 1060°-nm OCT system and further to the anatomic distance. This resulted in thickness maps for individual eyes. Reported variation for automatic segmentation in eyes with pathology is 13%,[23] comparable with values seen by retinal automated segmentation.[25]

A compound map showed a pixel-wise summary (either by averaging or by using the difference between maps) of the information in each individual thickness map at each location of

Investigative Ophthalmology & Visual Science

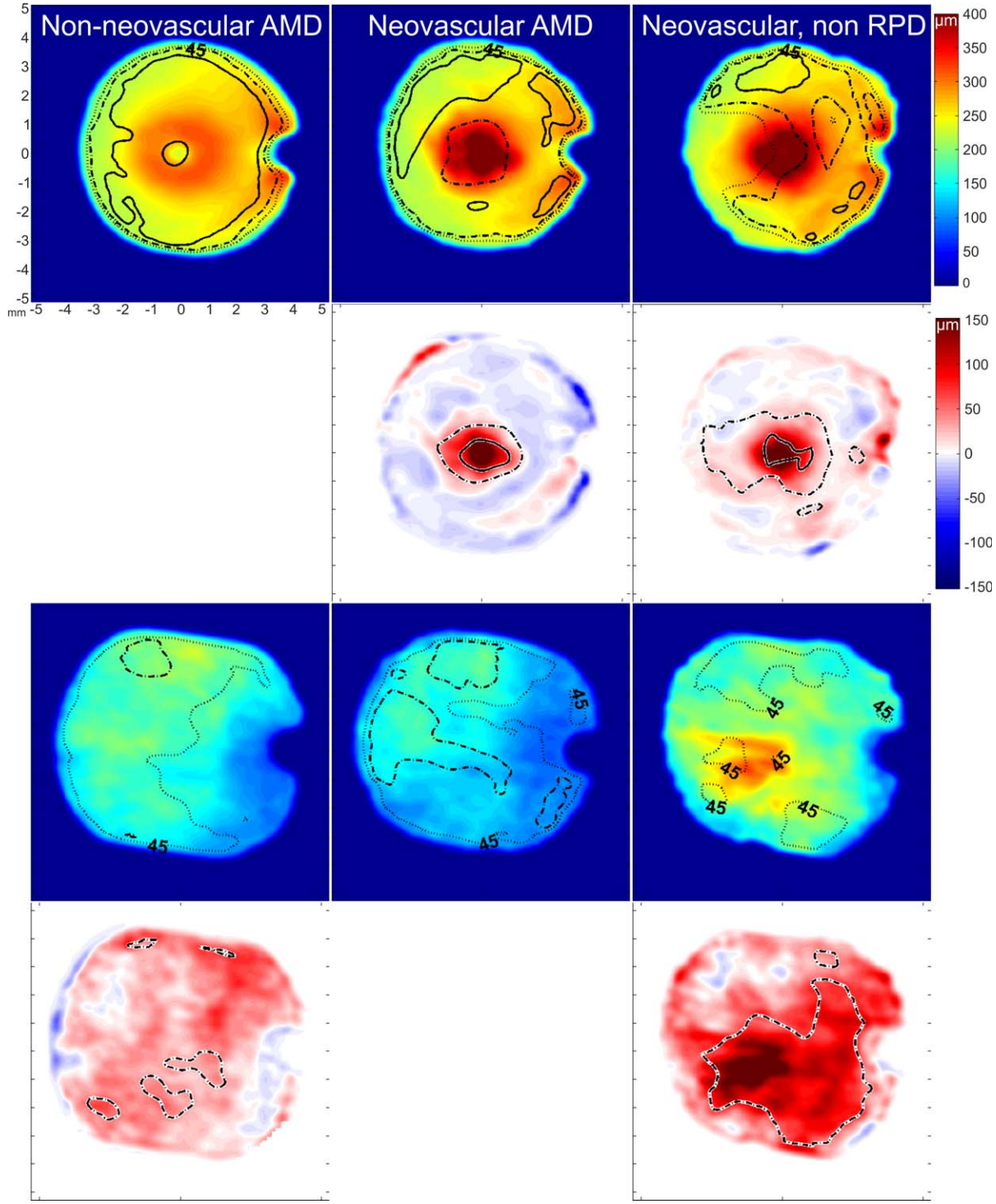

Figure 1. Average compound thickness maps for the retina (*first row*) and the choroid (*third row*). *Dotted*, *broken*, and *solid lines* represent 45%, 30%, and 15% variation, respectively. Difference maps for the retinal thickness analysis (*second row*) and for the choroidal thickness analysis (*fourth row*) show the amount and location of significant difference found by post hoc testing between groups. *Broken* and *solid contour lines* represent a significant difference of $P < 0.05$ and $P < 0.001$, respectively.

the map. This image analysis has been described in depth in a previous study.[24] Briefly, to create color-coded compound maps of average thickness, the mean and SD of retinal and choroidal thickness was obtained for each group of eyes. The coefficient of variation was used to map contour lines of 45%, 30%, and 15% on the compound map for the variation within each group. Difference maps were generated to investigate the change in thickness by subtracting each group from the other group. A further statistical analysis of the difference between each non-RPD and the RPD groups was generated by conducting *t*-tests over the field of view. To show areas of statistically significant difference between the compound maps, contour lines for *P* values smaller than 0.05 and 0.001 were drawn on the difference maps. Compound maps for the thickness difference

Investigative Ophthalmology & Visual Science

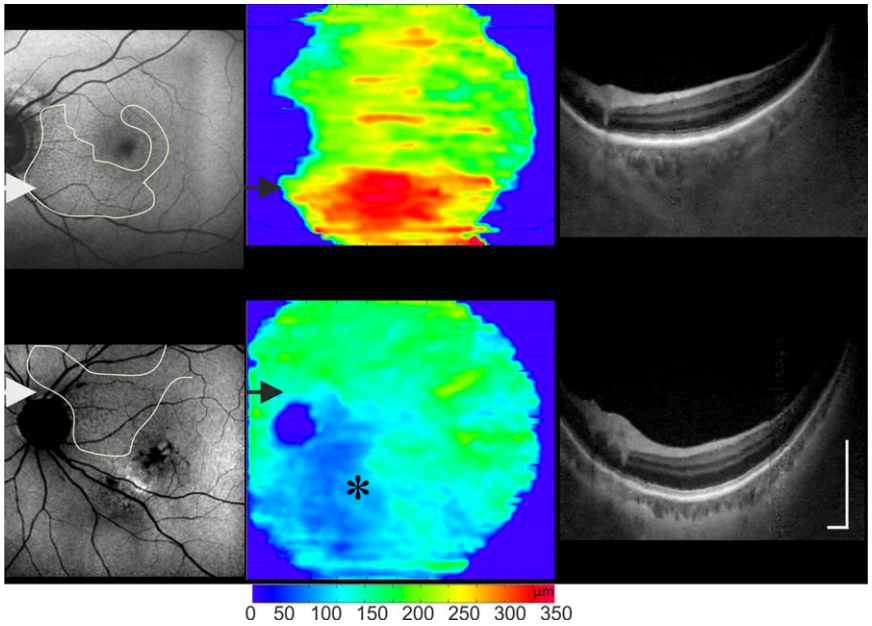

Figure 2. Reticular pseudodrusen and ChT distribution for three different examples: a nonneovascular AMD, neovascular AMD (the location of the CNV is marked with *) viewed on FAF, and 3D 1060-nm OCT ChT maps and OCT tomograms (location shown by the *arrows*). Areas with RPD correspond (*contour lines on FAF images*) to areas of increased ChT in each example. *Scale bar*: 0.5 mm.

shown in this article are only the maps with areas of significant statistical difference. To judge the clinical significance of possible ChT distribution within each study eye, ChT maps were compared with FAF images. For delineating visible RPD area, FAF images were used. Areas were delineated by two investigators independently before being compared with ChT distribution in maps to ensure a masked comparison. If delineated areas differed, the two investigators discussed their selection and agreed on overlapping areas as the final choice of RPD areas. For statistical analysis, subfoveal ChT measurement was located beneath the foveola and measured after automatic segmentation and smoothing for compound maps and controlled for manually by an experienced observer.

With a novel blood vessel segmentation algorithm, Sattler's and Haller's layer thicknesses were automatically determined.[26] The algorithm identifies the voxels that belong to vessels and plots them by the ratio of inner and outer vessels. Outer voxels are neighbored nonvessel voxels. This ratio determines vessel size, and large vessels (large ratio between inner and outer voxels) located closer to the sclera are assigned to Haller's layer, while vessels that are located above them and are smaller belong to Sattler's layer. Vessels' voxels equal or below resolution were interpreted as noise. The sublayer thickness was locally averaged based on the ETDRS grid that divides the macula into nine subfields. Measurements in eyes with AMD have a repeatability variation of 31% in the Haller's layer, which is comparable with automatic segmentation in healthy eyes and published manual segmentation methods.[27] When Sattler's layer becomes indistinct in eyes with AMD, the repeatability of the automatic segmentation is decreased. However, clinically, the actual thickness numbers are still within a very small range (e.g., the difference between 4 and 7 µm is 44%, but the absolute values are still very small).

The statistics software, IBM SPSS Statistics for Windows, Version 20.0 (IBM Corp., Armonk, NY, USA) was used for conducting ANOVA testing and multiple regression analysis of the contribution of groups and their characterizing factors to ChT.

Results

Eyes with RPD were grouped together according to the severity of their AMD into nonneovascular ($n = 26$) and neovascular AMD ($n = 11$). Remaining eyes with neovascular AMD that did not present with RPD were grouped together ($n = 10$). Three eyes with acquired vitelliform macular dystrophy were not included in the statistical analysis, leaving 47 eyes. The analysis of retinal and ChT foveally (Table 1) and over the field of view (Fig. 1) showed that while retinal thickness increase was following the severity of the AMD (with both groups of neovascular AMD being thickest), ChT was thinnest when RPD were present in the neovascular group. The difference between neovascular AMD eyes with and without RPD was evident throughout the compound maps, sparing the superior fundus. Multiple regression analysis showed also a significant contribution of age and axial eye length (AL) to ChT ($R^2 = 0.33$; $P < 0.001$; age: $\beta = -0.4$, $P < 0.01$; AL: $\beta = -0.4$, $P < 0.01$; AMD severities: $\beta = 0.24$, $P < 0.05$).

When comparing delineated RPD areas with the ChT maps, the thickest areas within each map were below the RPD regardless of the AMD severity. These areas had thicker choroids in relation to the overall ChT seen on each map. The choroid below the RPD area was thicker than below CNV (Fig. 2), GA (Fig. 3A), or accumulation of drusen (Fig. 3D).

With 3D 1060-nm OCT, RPD had the same appearance when compared with 800-nm OCT images at the same location (Fig. 4). On 3D 1060-nm OCT tomograms, RPD are represented as subretinal hyperreflective areas, superior to the RPE, with the thicker RPD with disturbances of the inner segment/outer segment line comparable with the RPD appearance on 800-nm OCT images. Small drusen and RPD can be differentiated reliably on all images. In non-CNV AMD, drusen were found in the center of the macula, while RPD were located in the macula periphery (Fig. 3). Choroidal neovascularization was found within the macular area. Reticular pseudodrusen were mostly distributed superiorly (Table 1).

Sattler's and Haller's layer thickness measurements and differences between AMD severities are presented in Table 2. In three subfields Sattler's layer was significantly thicker in the

Investigative Ophthalmology & Visual Science

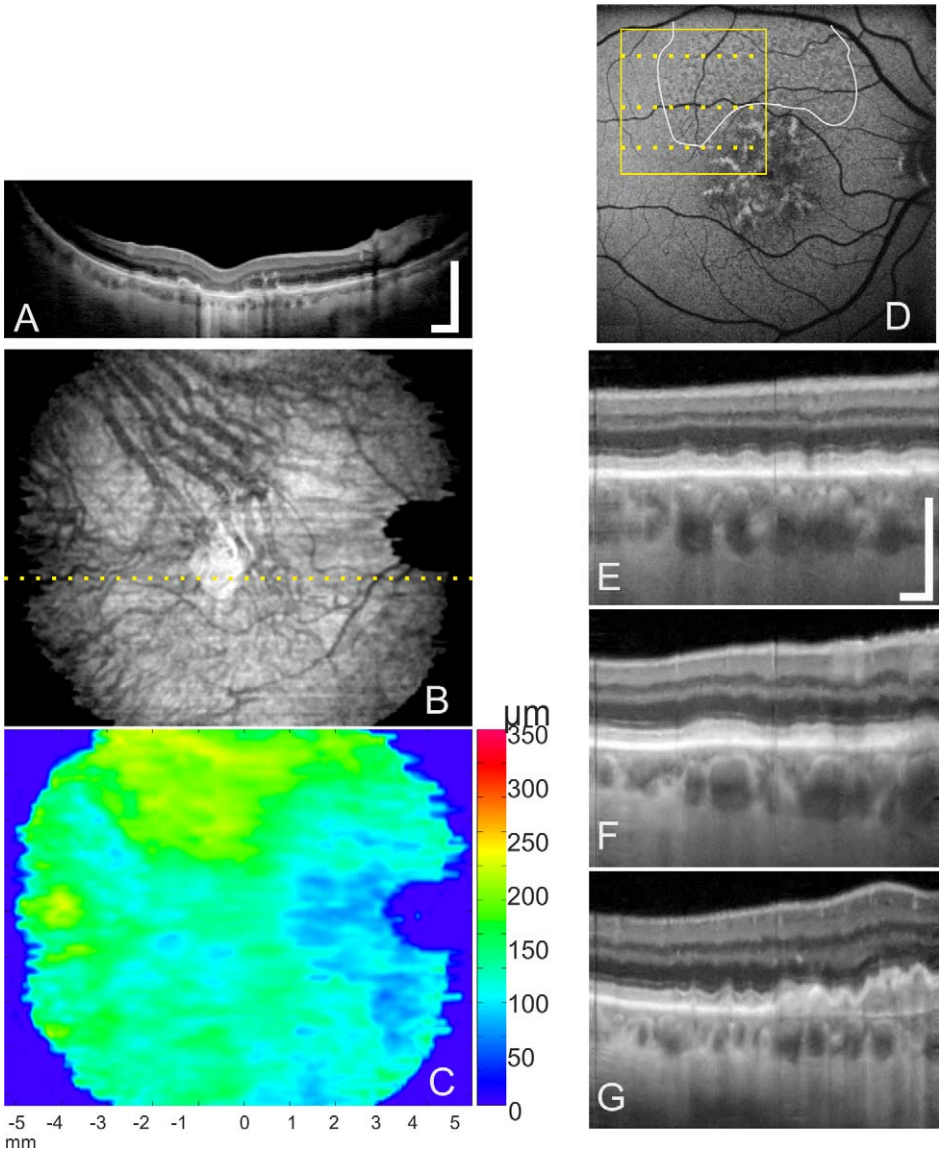

Figure 3. Reticular pseudodrusen and drusen appearance according to macular location in 3D 1060-nm OCT. (**A**) Tomogram through the foveal area (*dotted line* in [**B**]), displaying geographic atrophy. (**B**) Enface of 1060-nm OCT averaged through the choroid. (**C**) Color map visualizing the distribution of ChT. Thickest area is located superiorly, agreeing with the large dense RPD area. (**D**) Fundus autofluorescence images with locations of RPD accumulation identified by two investigators (*white contour line*) and enlarged area (*yellow box*) of OCT tomograms. (**E**–**G**) Tomograms showing details of drusen and RPD deposits in relation to their proximity to the fovea. Scale bars: 0.5 mm.

group with neovascular eyes and no RPD (central, inner and outer inferior subfields). Haller's layer was more often significantly thicker in neovascular eyes with RPD beside in the superior inner and outer fields and in the temporal outer field. The absolute Sattler's thickness was very low so that, proportionally, Haller's layer made up most of the vessels seen in the choroid in the two groups with RPD, while the proportional difference between Haller's and Sattler's layer was much smaller in the group without RPD.

Discussion

The current study examined ChT alterations related to AMD severity and the presence of RPD. The central and inferior choroids, including Sattler's and Haller's layers, were thicker in eyes without RPD. In eyes with RPD, ChT was greater in areas with RPD than in areas without RPD within each eye. Thus, the presence of RPD in an eye tended to skew ChT markedly, with ChT greater in areas where RPD were present and also thinner in those areas where RPD were not present. Marked thinning of Sattler's layer to median single-digit micrometer thicknesses was found in almost all regions of all eyes with RPD, whether neovascular or not (Table 2). These findings, as demonstrated by spatial mappings generated from high-density OCT scans, are not only more specific and detailed but also consistent with prior investigations reporting higher mean ChT in eyes without AMD or RPD.[15,16] Querques et al.[15] found a thicker choroid at 3000 μm superior to the fovea with a mean of 187.2 ± 9.5 μm and subfoveally 176.4 ± 10.1 μm, respectively, but both were not thicker than controls with early AMD and no RPD. In the controls, ChT was greatest at the fovea 241.5 ± 16.5 μm and less at 3000 μm superior to the fovea 210.5 ± 11.8 μm. In another study, eyes with RPD regression showed a stronger choroidal thinning over time than those without regression.[6] In

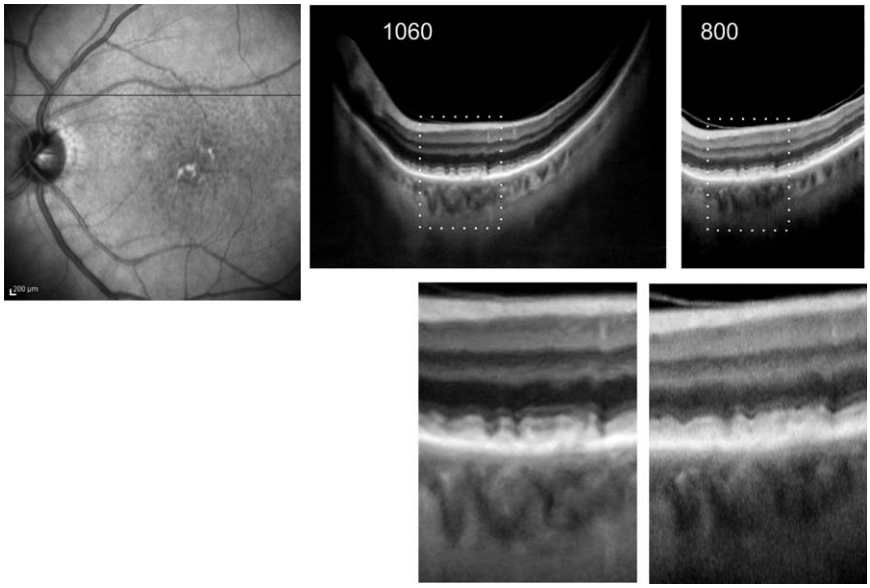

Figure 4. Comparison of OCT modalities between OCT tomograms at 1060 nm (36° field of view) and at 800 nm (20° field of view), taken from a scanned volume at the same location (*line on the FAF image*, *left*) and enlarged views (*bottom*).

agreement with the current study, the non-RPD eyes of both studies[6,15] had thicker choroids than eyes with RPD.

Several factors were found to contribute to ChT. Age and AL have also a negative correlation with ChT in healthy eyes.[24,28,29] The fact that AMD severity is codetermining the base ChT may be explained by the finding that AMD with RPD shares the same major genetic factors as AMD without RPD.[30] Reticular pseudodrusen had a localized effect, which may have weakened its combined contribution. In an analysis of individual eyes, areas with RPD were associated with thicker choroid beneath them. Since most RPD were found superiorly, this may explain the insufficient statistical significant decrease in ChT in this location in the compound map analysis (Fig. 1).

Inflammation has been suggested to be consistent with the appearance of RPD lesions.[31] Fibrosis and atrophy have been suggested to result from RPD presence.[10,14,15] Possibly, the presence of RPD in the eye marks a more severe disease pathogenesis with RPD-associated inflammation increasing the ChT, and the overall ChT decrease is a result of following fibrosis and atrophy. In this study cohort, the AMDs were advanced, and it remains to clarify if possible inflammation is only locally active or if the choroid was mechanically too rigid to thicken globally. Histologic marking in fresh sections with and without RPD could result in a conclusive determination of inflammation.

The use of OCT has been recommended for the detection and classification of drusen and RPD.[32] In the present study, it was possible to segment and correlate vessel distribution owing to the ability of 3D 1060-nm OCT to accurately visualize ChT and vasculature. Choroidal thickness mapping has been shown to locate regional changes in diabetic eye disease[33] and adds another useful investigational tool for AMD. Vessel analysis confirmed that ChT differences in RPD colocalize with the RPD lesions themselves and that thickness changes involve both Sattler's and Haller's layers of the choroid. Total

Table 2. Automatically Segmented Mean Sattler's and Haller's Layer Thickness Across the Early Treatment Diabetic Retinopathy Study Grid Subfields (Mean ± SD, Median)

	Sattler's Layer			Haller's Layer		
AMD Severities	**Nonneovascular With RPD**	**Neovascular With RPD**	**Neovascular With No RPD**	**Nonneovascular With RPD**	**Neovascular With RPD**	**Neovascular With No RPD**
Central submacular*†	25 ± 33, 8	12 ± 17, 6	59 ± 47, 48	73 ± 28, 80	64 ± 25, 54	130 ± 57, 121
Superior inner	26 ± 35, 8	11 ± 17, 8	50 ± 49, 35	81 ± 39, 60	70 ± 49, 52	119 ± 67, 104
Temporal inner†	21 ± 28, 7	11 ± 18, 6	49 ± 51, 27	79 ± 36, 63	61 ± 26, 53	115 ± 61, 100
Inferior inner*†	23 ± 36, 7	12 ± 20, 4	68 ± 48, 48	74 ± 34, 61	59 ± 19, 51	135 ± 64, 139
Nasal inner†	26 ± 33, 11	14 ± 21, 6	57 ± 46, 53	75 ± 37, 56	64 ± 29, 54	131 ± 62, 150
Superior outer	21 ± 25, 10	8 ± 7, 5	36 ± 35, 21	79 ± 37, 61	67 ± 37, 55	111 ± 66, 96
Temporal outer	16 ± 22, 5	8 ± 7, 6	29 ± 30, 12	73 ± 31, 57	60 ± 22, 50	103 ± 68, 80
Inferior outer*†	15 ± 20, 8	8 ± 9, 4	48 ± 37, 56	69 ± 27, 59	63 ± 22, 51	118 ± 55, 119
Nasal outer†	19 ± 25, 8	12 ± 16, 6	42 ± 31, 46	69 ± 28, 56	63 ± 29, 50	118 ± 53, 137

Data are expressed as mean ± SD in micrometers.

* $P < 0.05$, Kruskal-Wallis test, when compared between the disease groups for each sublayer.

† $P < 0.05$ with a significant difference between the neovascular group without RPD and the other groups with RPD (one-way ANOVA, post hoc $P < 0.05$).

Investigative Ophthalmology & Visual Science

choroidal and sublayer thickness may enable proposed sensitive investigation of regional choroidal thicknesses in relation to the state of RPD life cycle.[6]

In conclusion, 3D 1060-nm OCT tomograms visualize identical RPD or subretinal deposits above the RPE as seen with commercial OCT systems at 800 nm, while enabling the analysis of densely scanned volumes over a large field of view. The present study investigated retinal and choroidal thickness mapping with this technology and showed that ChT in AMD patients with RPD decreased generally with increasing AMD disease severity and locally increased within each eye in correlation with the RPD lesions themselves. The presence of RPD was associated with marked thinning of Sattler's layer throughout, a new finding that may shed light on the relationship of RPD with the choroid.

Acknowledgments

The authors thank Aneesh Alex and the staff of the Macula Clinic at the Rudolf Foundation Clinic for their valuable support throughout the study.

Supported in part by Medical University Vienna, Macular Vision Research Foundation (MVRF; West Conshohocken, PA, USA), European Union Project FUN OCT (FP7 Health, Contract No. 201880), FAMOS (FP7 ICT 317744), FWF-NFN "Photoacoustic imaging in biology and Medicine," Oesterreichische Nationalbank (Jubiläumsfond, Project No. 14294), National Institutes of Health (NIH R01-EY011289-27), Carl Zeiss Meditec, Inc., Femtolasers GmbH, and the Christian Doppler Society (Christian Doppler Laboratory "Laser development and their application in medicine").

Disclosure: **P. Haas**, None; **M. Esmaeelpour**, None; **S. Ansari-Shahrezaei**, None; **W. Drexler**, Carl Zeiss Meditec (C); **S. Binder**, None

References

1. Smith RT, Sohrab MA, Busuioc M, Barile G. Reticular macular disease. *Am J Ophthalmol*. 2009;148:733–743.
2. Spaide RF, Curcio CA. Drusen characterization with multimodal imaging. *Retina*. 2010;30:1441–1454.
3. Age-Related Eye Disease Study Research Group. A randomized, placebo-controlled, clinical trial of high-dose supplementation with vitamins C and E, beta carotene, and zinc for age-related macular degeneration and vision loss: AREDS report No. 8. *Arch Ophthalmol*. 2001;119:1417–1436.
4. Ferris FL III, Wilkinson CP, Bird A, et al. Clinical classification of age-related macular degeneration. *Ophthalmology*. 2013; 120:844–851.
5. Mimoun G, Soubrane G, Coscas G. Macular drusen [in French]. *J Fr Ophtalmol*. 1990;13:511–530.
6. Spaide RF. Outer retinal atrophy after regression of subretinal drusenoid deposits as a newly recognized form of late age related macular degeneration. *Retina*. 2013;33:1800–1808.
7. Zweifel SA, Spaide RF, Yannuzzi LA. Acquired vitelliform detachment in patients with subretinal drusenoid deposits (reticular pseudodrusen). *Retina*. 2011;31:229–234.
8. Schmitz-Valckenberg S, Alten F, Steinberg JS, et al. Reticular drusen associated with geographic atrophy in age-related macular degeneration. *Invest Ophthalmol Vis Sci*. 2011;52: 5009–5015.
9. Xu L, Blonska AM, Pumariega NM, et al. Reticular macular disease is associated with multilobular geographic atrophy in age-related macular degeneration. *Retina*. 2013;33:1850–1862.
10. Arnold JJ, Sarks SH, Killingsworth MC, Sarks JP. Reticular pseudodrusen: a risk factor in age-related maculopathy. *Retina*. 1995;15:183–191.
11. Pumariega NM, Smith RT, Sohrab MA, Letien V, Souied EH. A prospective study of reticular macular disease. *Ophthalmology*. 2011;118:1619–1625.
12. Cohen SY, Dubois L, Tadayoni R, Delahaye-Mazza C, Debibie C, Quentel G. Prevalence of reticular pseudodrusen in age-related macular degeneration with newly diagnosed choroidal neovascularisation. *Br J Ophthalmol*. 2007;91:354–359.
13. Switzer DW Jr, Mendonça LS, Saito M, Zweifel SA, Spaide RF. Segregation of ophthalmoscopic characteristics according to choroidal thickness in patients with early age-related macular degeneration. *Retina*. 2012;32:1265–1271.
14. Sohrab MA, Smith RT, Salehi-Had H, Sadda SR, Fawzi AA. Image registration and multimodal imaging of reticular pseudodrusen. *Invest Ophthalmol Vis Sci*. 2011;52:5743–5748.
15. Querques G, Querques L, Forte R, Massamba N, Coscas F, Souied EH. Choroidal changes associated with reticular pseudodrusen. *Invest Ophthalmol Vis Sci*. 2012;53:1258–1263.
16. Alten F, Clemens CR, Heiduschka P, Eter N. Localized reticular pseudodrusen and their topographic relation to choroidal watershed zones and changes in choroidal volumes. *Invest Ophthalmol Vis Sci*. 2013;54:3250–3257.
17. Sohrab M, Wu K, Fawzi AA. A pilot study of morphometric analysis of choroidal vasculature in vivo, using en face optical coherence tomography. *PLoS One*. 2012;7:e48631.
18. Schmitz-Valckenberg S, Steinberg JS, Fleckenstein M, Visvalingam S, Brinkmann CK, Holz FG. Combined confocal scanning laser ophthalmoscopy and spectral-domain optical coherence tomography imaging of reticular drusen associated with age-related macular degeneration. *Ophthalmology*. 2010;117: 1169–1176.
19. Age-Related Eye Disease Study Research Group. The Age-Related Eye Disease Study system for classifying age-related macular degeneration from stereoscopic color fundus photographs: the Age-Related Eye Disease Study report number 6. *Am J Ophthalmol*. 2001;132:668–681.
20. ANSI Z136 Committee. *Safe Use of Lasers and Safe Use of Optical Fiber Communications*. Washington, DC: American National Standards Institute; 2000:168.
21. ICNIRP. *Revision of the Guidelines on Limits of Exposure to Laser Radiation of Wavelengths Between 400nm and 1.4μm*. Oberschleissheim, Germany: International Commission on Non-Ionizing Radiation Protection; 2000:431–440.
22. Rasband WS. *ImageJ*. Bethesda, MD: National Institutes of Health;1997–2012.
23. Kajić V, Esmaeelpour M, Považay B, Marshall D, Rosin PL, Drexler W. Automated choroidal segmentation of 1060 nm OCT in healthy and pathologic eyes using a statistical model. *Biomed Opt Express*. 2011;3:86–103.
24. Esmaeelpour M, Povazay B, Hermann B, et al. Three-dimensional 1060nm OCT: choroidal thickness maps in normals and improved posterior segment visualization in cataract patients. *Invest Ophthalmol Vis Sci*. 2010;51:5260–5266.
25. Kajić V, Povazay B, Hermann B, et al. Robust segmentation of intraretinal layers in the normal human fovea using a novel statistical model based on texture and shape analysis. *Opt Express*. 2010;18:14730–14744.
26. Kajić V, Esmaeelpour M, Glittenberg C, et al. Automated three-dimensional choroidal vessel segmentation of 3D 1060 nm OCT retinal data. *Biomed Opt Express*. 2013;4:134–150.
27. Sim DA, Keane PA, Mehta H, et al. Repeatability and reproducibility of choroidal vessel layer measurements in diabetic retinopathy using enhanced depth optical coherence tomography. *Invest Ophthalmol Vis Sci*. 2013;54:2893–2901.
28. Ikuno Y, Kawaguchi K, Yasuno Y, Nouchi T. Choroidal thickness in healthy Japanese subjects. *Invest Ophthalmol Vis Sci*. 2009;51:2173–2176.

29. Margolis R, Spaide RF. A pilot study of enhanced depth imaging optical coherence tomography of the choroid in normal eyes. *Am J Ophthalmol*. 2009;147:811–815.
30. Puche N, Blanco-Garavito R, Richard F, et al. Genetic and environmental factors associated with reticular pseudodrusen in age-related macular degeneration. *Retina*. 2013;33:998–1004.
31. Smith RT, Chan JK, Busuoic M, Sivagnanavel V, Bird AC, Chong NV. Autofluorescence characteristics of early, atrophic, and high-risk fellow eyes in age-related macular degeneration. *Invest Ophthalmol Vis Sci*. 2006;47:5495–5504.
32. Zweifel SA, Imamura Y, Spaide TC, Fujiwara T, Spaide RF. Prevalence and significance of subretinal drusenoid deposits (reticular pseudodrusen) in age-related macular degeneration. *Ophthalmology*. 2010;117:1775–1781.
33. Esmaeelpour M, Brunner S, Ansari-Shahrezaei S, et al. Choroidal thinning in diabetes type 1 detected by 3-dimensional 1060 nm optical coherence tomography. *Invest Ophthalmol Vis Sci*. 2012;53:6803–6809.

Investigative Ophthalmology & Visual Science